JOURNAL OF CATALYSIS 89, 20–34 (1984)

Synthesis, Characterization, and Fischer–Tropsch Studies of Iron-Containing Zeolites

STEVEN L. SUIB,*[,1] KERRY C. MCMAHON,* LI MIN TAU,† AND CARROLL O. BENNETT†

*Department of Chemistry and Institute of Materials Science and †Department of Chemical Engineering, University of Connecticut, Storrs, Connecticut 06268

Received October 18, 1983; revised April 16, 1984

Iron has been incorporated into several zeolites with adsorption, ion-exchange, and anionic complexation procedures. These samples have been reduced in flowing hydrogen at temperatures between 300 and 500°C. Particle size measurements using X-ray powder diffraction and electron microscopy techniques reveal that all of the iron phases of the reduced samples are between 50 and 150 Å. Changes in the catalysts due to their interactions with 10% CO/H_2 at temperatures ranging from 260 to 400°C were determined by Mössbauer spectroscopy using an *in situ* cell. Catalytic activity was monitored by a gas chromatograph and quantitative analysis of the product distribution was done in a separate differential reactor which was interfaced to a mass spectrometer. Alloy formation was not observed.

INTRODUCTION

Recently there has been much interest in preparing highly dispersed and reduced iron (0) species in several catalytic materials like zeolites (*1–6*). Mössbauer studies (*1, 37*) of iron-containing zeolites have recently been reviewed (*8*). None of these studies has involved the use of an *in situ* treatment cell.

Ballivet-Tkatchenko and co-workers (*4, 9*) have studied $Fe(CO)_5$, $Fe_2(CO)_9$, and $Fe_3(CO)_{12}$ by infrared (*9*), and catalytic (*4*) methods. Most of the interest regarding catalysis by these iron-containing zeolites centers around the Fischer–Tropsch reaction. Several mechanisms for this reaction (*10*) have been suggested. Deviations from Schulz–Flory kinetic distributions have been reported (*12, 13*).

The purpose of our work is to report the activity, selectivity, and stability of $Fe(CO)_5$ and bimetallic zeolite catalysts. These catalysts have all been studied with Mössbauer spectroscopy and with the transient pulse technique (*14*). Several other spectroscopic measurements have been made to ascertain the effects of the chemical composition of the catalysts before, during, and after reaction.

The results of these studies suggest that the $Fe(CO)_5$ and bimetallic zeolite catalysts consist of large iron particles on the surface of the zeolite. Researchers at Mobil (*31*) have shown that physically separating the zeolite component from the Fischer–Tropsch component such as the samples studied here is a viable and attractive route. The surface states of these zeolite catalysts can be studied with the transient pulse method.

EXPERIMENTAL METHODS

A. Mössbauer Studies

The description of the Mössbauer system can be found elsewhere (*8*).

B. Transient Pulse Methods

The transient pulse experiments described here involve atmospheric pres-

[1] To whom all correspondence should be addressed.

0021-9517/84 $3.00

TABLE 1

Sample	Metal	Fe component	Support	Reduction condition
1	[a]	$Fe(CO)_5$	NaY	450°C, 75 ml/min H_2, 24 hr
2	Cu^{2+}	$Na_2Fe(CN)_5NO$	ZSM-5	400°C, 75 ml/min H_2, 4 hr
3	Zn^{2+}	$Na_2Fe(CN)_5NO$	NH_4Y	400°C, 75 ml/min H_2, 4 hr
4	Co^{2+}	$Na_2Fe(CN)_5NO$	NH_4Y	400°C, 75 ml/min H_2, 4 hr
5	Ru^{3+}	$Na_2Fe(CN)_5NO$	NH_4Y	400°C, 75 ml/min H_2, 4 hr

[a] No other metal used.

sure gas phase methods. Step functions, pulses and square waves are generated with a low volume chromatographic four-way valve. Switching valves are used to rapidly change the gas mixtures. The catalyst is placed in a differential reactor. A four-way valve at the outlet of the reactor directs gases to the mass spectrometer. Further details and results of this method can be found elsewhere (*14, 37, 38*).

The transient pulse method (*14*) was used to study the reaction of 10% CO/H_2 mixtures with iron-containing zeolites. Typically, 25 mg of zeolite was pelletized and loaded into a catalytic reactor (*14*). Samples were treated according to conditions in Table 1. The catalysts were purged with helium gas and mixtures of 10% CO/H_2 were passed over the zeolites (30 ml/min) at temperatures between 285 and 450°C. Product distributions were monitored with a cycloidal mass spectrometer, model CEC 21621. The output of the mass spectrometer is continuous in time, but points are shown in some of the figures in order to identify the various products.

C. Sample Preparation

Reagents. Zeolites NH_4Y and NaY were obtained in a powdered form from the Linde Division of Union Carbide. The NaY was under the code SK-40 and lot number #042578. The NH_4Y (SK-41) had a lot number #042578. Zeolite ZSM-5 was prepared by mixing colloidal silica, tetrapropyl ammonium bromide, sodium aluminate, and sodium hydroxide and treating this mixture in an autoclave at 175°C for 8 days as described in a patent by Argauer and Landolt (*23*). The particular procedure of this patent that was followed was example 27. The $Fe(CO)_5$ was purchased from the ALFA Co, lot #091179, which is 99.5% pure. All water that was used for ion-exchange purposes was distilled and then deionized. The transition metal coordination complex $Na_2Fe(CN)_5NO$ (sodium nitroprusside) was purchased from the J. T. Baker Chemical Company lot #52848. The Cu^{2+}, Zn^{2+}, and Co^{2+} ions were ion-exchanged from solutions of $Cu(NO_3)_2 \cdot 6H_2O$, $Zn(NO_3)_2 \cdot 6H_2O$, and $Co(NO_3)_2 \cdot 6H_2O$, respectively. The copper and cobalt salts were purchased from the General Chemical Division of Allied Chemical and Dye Corporation, lot #W030 (Cu^{2+}) and lot #H018 (Co^{2+}). The zinc was from Fischer Scientific, lot #791947.

Samples: Sample 1. $Fe(CO)_5$ was introduced into NaY zeolite by taking 0.13 ml of $Fe(CO)_5$ (0.19 g) and placing this in one side of an inverted U-tube with a syringe. The $Fe(CO)_5$ was immediately frozen and then 1 g of NaY zeolite was added to the other side of the tube. This U-tube was then connected to a vacuum line and evacuated to a pressure less than 1×10^{-5} atm. while the $Fe(CO)_5$ was still frozen. The tube was then isolated from the vacuum line by closing a stopcock and the $Fe(CO)_5$ was allowed to slowly distill onto the zeolite. This distillation procedure was complete after 5 min. This material had a variety of colors ranging from yellow to orange brown depending on the volume of $Fe(CO)_5$ used in the prep-

aration. The sample studied in this investigation initially had a yellow color.

Sample 2–4. One gram of zeolite was added to 100 ml of 10% transition metal solution and ion-exchanged for 1 hr at 90°C while stirring. The mixtures were then filtered, washed with distilled deionized water, and dried. The resultant solids were complexed with 100 ml of 10% aqueous sodium nitroprusside solution. The mixtures were filtered, washed, and dried on a vacuum line to a pressure of 1×10^{-3} atm. All samples were stored in capped vials sealed with parafilm, a wrapping film from Fischer Scientific.

Sample 5. The $Ru(NH_3)_6Br_3$ was prepared by reacting $[Ru(NH_3)_6]Cl_2$ with Br_2 and NaBr according to procedures described by Fergusson and Love (*24*). Fifty milliliters of a 0.05 *M* solution of $[Ru(NH_3)_6]Br_3$ was added to 1 g of NH_4Y zeolite and stirred under nitrogen for 21 hr. This resulted in a gray product after filtration, washing, and drying. This material was then dehydrated at 150°C under vacuum for one hour and then complexed with 100 ml of a 10% aqueous solution of $Na_2Fe(CN)_5NO$ for 6 hr at room temperature. The final product was violet in color.

D. Supporting Spectroscopy and Characterization Methods

1. X-ray powder diffraction. X-Ray powder diffraction data were collected with a Diano-XRD 8000 X-ray powder diffraction instrument. Samples were mounted on glass slides that had a slight coating of vaseline on the surface.

2. Infrared methods. Infrared spectra of the $Fe(CO)_5$ and bimetallic zeolite samples were collected on a Model 283 Perkin Elmer spectrometer. Self supporting wafers of the zeolite were made and placed in an all glass *in situ* infrared cell which was placed in the spectrometer.

3. Ion scattering and secondary ion mass spectrometry. Surface analyses of the bimetallic zeolites were carried out on hydrated and dehydrated samples. Further details concerning the experimental conditions, data manipulation, limitations, and potential uses of these methods to zeolites have been reported in greater detail elsewhere (*18*).

4. Electron microscopy. Transmission electron microscopy experiments were performed on a model HU200 Hitachi transmission electron microscope. Samples were prepared by dispersing the zeolites into methanol in a vial. The vial was then immersed in an ultrasonic vibration apparatus. After ultrasonic vibration, one drop of a methanol mixture was placed on a carbon coated 300 mesh copper grid.

5. X-ray photoelectron spectroscopy experiments. X-Ray photoelectron spectroscopy measurements of these zeolites were carried out by making a pellet of the zeolite samples and mounting the solid with a conducting epoxy to the sample holder. Analyses were done with a KRATOS XSAM 800 electron spectrometer using a Mg$K\alpha$ X-ray source. Data were analyzed on a PDP 11/03 central processor by using fast fourier transform resolution enhancement, peak synthesis, satellite subtraction, background subtraction, and peak determination methods.

RESULTS

A. Sample Preparation and Mössbauer Studies

The different metals, zeolite supports, iron components, and reduction conditions for the five samples investigated here are outlined in Table 1. For clarity the samples will be referred to as samples 1 through 5.

As observed in Table 1, samples 2 through 5 are bimetallic zeolite catalysts and sample 1 contains only iron. These samples have been prepared by three main procedures. These procedures are ion-exchange, sublimation, and transition metal anion coordination. One of our main interests is to investigate the preparation method of Scherzer and Fort (*2*). The object here is to see how general the method

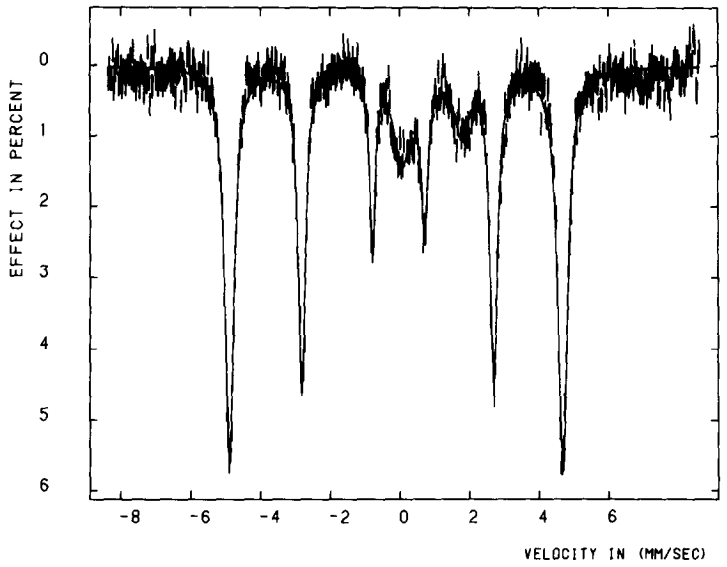

FIG. 1. Mössbauer spectrum of $CoNH_4Y$ zeolite after reduction, 400°C, 75 ml/min H_2, 4 hr.

is, how the anion complex interacts with the cation and if complexation occurs only on the exterior of the zeolite crystallites or if complexation in the pores has occurred. Several other metals and zeolite supports and the results of these studies can be found elsewhere (*8*).

Ideal reduction conditions for these 5 samples were determined by Mössbauer spectroscopy and are reported in Table 1. For instance, all 5 samples were thermally treated at several temperatures between 100 and 500°C and under several different flow rate conditions of hydrogen (30–75 ml/min). The conditions reported in Table 1 are those that are the lowest temperatures and lowest hydrogen flow rates necessary to reduce the iron to the metallic state. Iron Mössbauer experiments were used to deduce the degree of reduction and to ascertain which reduction conditions were desirable.

The Mössbauer spectrum of cobalt exchanged NH_4Y (sample 4) zeolite complexed with sodium nitroprusside after reduction is shown in Fig. 1. These conditions are the lowest temperatures, flow rates, and time for reduction of the $Fe(CN)_5NO^{2-}$ to alpha-iron. The corresponding Mössbauer spectrum of sample 1 that has been reduced is shown in Fig. 2.

The data in Table 2 were obtained from Mössbauer spectroscopy experiments. Samples 1–5 were analyzed before and after reduction. The values before reduction of the isomer shift, δ(mm/sec), and the quadrupole splitting, ΔE_Q(mm/sec), isomer shift, and the hyperfine field strength, H(kOe), after reduction are listed for each sample. No signal was observed for the ruthenium NH_4Y nitroprusside complex, sample #5.

Mössbauer experiments of these and other zeolites (*8*) show that before reduction the anionic iron complex is present and the Mössbauer isomer shifts and quadrupole splittings are very similar but slightly shifted from the uncomplexed anionic salt systems. However, we note here that unless a d-block transition metal is used as the cationic form of the zeolite there is no complexation of the iron anionic group as indicated by microanalysis and by Mössbauer spectroscopy (*8*). For example, if alkali metal ions are the only ions present, after reaction with the nitroprusside or with hexa-

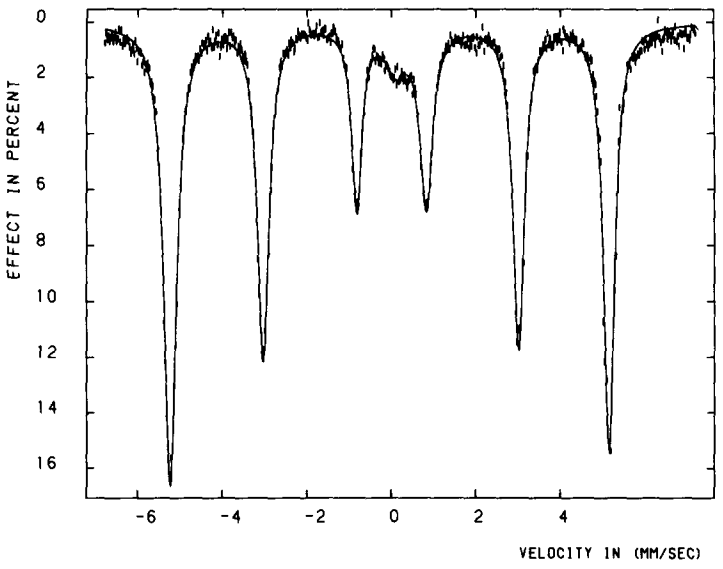

FIG. 2. Mössbauer spectrum of $Fe(CO)_5$/Y zeolite after reduction, 450°C, 75 ml/min H_2, 24 hr.

cyanoferrate (II) or (III) complexes, no iron incorporation in the zeolite is observed. If the transition metal ion is in an oxidation state higher than II there is little or no complexation.

Semiquantitative analyses obtained from energy and wavelength dispersive X-ray analyses and from atomic absorption spectroscopy were used to obtain information regarding bulk chemical composition. Sample 1 was 4.7% by weight iron. Sample 2 was 1.1 wt% iron and 1.8 wt% copper. Sample 3 was 5 wt% iron and 7 wt% zinc. Sample 4 was 3.4 wt% iron and 5.4 wt% cobalt. Sample 5 was 6 wt% ruthenium and 0.2 wt% iron. Estimates of the weight percent of iron from Mössbauer experiments are in good agreement with these analyses.

TABLE 2

Sample	As prepared		After reduction	
	δ(mm/sec)	ΔE_Q(mm/sec)	δ(mm/sec)	H(kOe)
1	0.40	1.0	−0.01	333.0
2	−0.20	1.8	−0.03	323.5
3	−0.20	1.8	0.03	320.4
4	−0.20	1.9	0.00	331.3
5	[a]	[a]	[a]	[a]

[a] No signal observed.

The most easily and completely reduced bimetallic zeolite samples using these procedures are the zinc complexes of nitroprusside and potassium hexacyanoferrate (III) and copper complexes of nitroprusside in zeolite Y. On the basis of ir, ISS-SIMS, and Mössbauer experiments nitroprusside complexation to copper ions in zeolite ZSM-5 also occurs, although reduction to alpha-iron is not complete. The ZSM-5 sample needed to be pretreated to 400°C in air for 30 min before being reduced in order to calcine carbonaceous material.

B. Other Spectroscopic Investigations

Each of the five samples was investigated by other spectroscopic measurements besides Mössbauer spectroscopy. All of the samples were studied with infrared spectroscopy, X-ray powder diffraction, and ion-scattering spectroscopy (ISS)/secondary ion mass spectrometry (SIMS). The characteristic infrared vibrational frequencies for the CO, CN^-, and NO functional groups for each sample are listed in Table 3. The qualitative results of the X-ray powder diffraction analyses as regards the crystalline nature of the material after reduction

TABLE 3

Sample	Infrared[a] (cm^{-1})	XRD[b]	ISS-SIMS[b,c]
1	2120, 2052, 2019, 1985, 1960	[d,e]	Fe
2	2205, 1950	[d,e]	Cu,[f] Fe
3	2205, 1950	[d,e]	Zn, Fe
4	2205, 1950	[d,e]	Co, Fe
5	2205, 1950	[d]	Ru, Fe[f]

[a] As prepared.
[b] Reduced samples according to conditions of Table 1.
[c] Transition metals present.
[d] Crystalline after reduction.
[e] α-Fe observed at 44.28°2θ.
[f] Minute amounts detected.

and the presence of α-Fe are also given in Table 3. The ISS-SIMS data indicate which transition metals were observed. Depth profiling experiments of these powders by ISS-SIMS (*18*) methods do not indicate any significant segregation of the two metals or any large concentration gradients. The ISS-SIMS data as reported in Table 3 indicate that samples 2 through 5 are indeed systems containing at least two different metals. There is no evidence from these experiments that alloys have formed. This is consistent with other spectroscopic measurements (Mössbauer) also reported here.

There are certainly other ir frequencies, other X-ray powder diffraction peaks, and ISS-SIMS data for other elements and groups of samples 1–5 that have not been reported here. These other data mainly deal with the aluminosilicate lattice.

Other experiments that were performed to identify what happened to the metal ions after reduction and reaction include electron microscopy and X-ray photoelectron spectroscopy experiments. X-Ray powder diffraction experiments and electron microscopy experiments indicate that there are large particles of alpha-iron after reduction of the bimetallic zeolites. These particles are smaller (50–80 Å) than the reduced $Fe(CO)_5$ zeolite samples (70–100 Å). Sample 2 was also studied with X-ray photoelectron spectroscopy after it was reduced. The signal for copper was very weak and when quantitatively analyzed yielded 0.2% copper. In addition, the Cu L_3VV Auger transition occurred at 918 eV and the Cu $2p_{3/2}$ transition was calculated to be at 932 eV.

C. Fischer–Tropsch Reactions

Samples 1–5 were used as Fischer–Tropsch catalysts and studied with the transient pulse method in a differential reactor. Sample 1 was heated at 150°C for 1 hr in helium (30 ml/min) followed by reduction with flowing hydrogen (75 ml/min) for 24 hr at 450°C. The temperature was then lowered to 285°C while decreasing the hydrogen flow to a rate of 30 ml/min. Then this catalyst was purged with helium for 3 min. After the helium purge a 10% CO/H_2 (30 ml/min) gas mixture was passed over the catalyst for 1 min. The product distribution for this reaction is given in Fig. 3. There is a 10.5% conversion of CO here. The amount of CH_4 being produced increases as reaction time continues as shown in Fig. 4. The reaction mixture was passed over sample 1 for a little more than 6 min.

In order to learn more about the surface active sites the catalyst can be titrated with

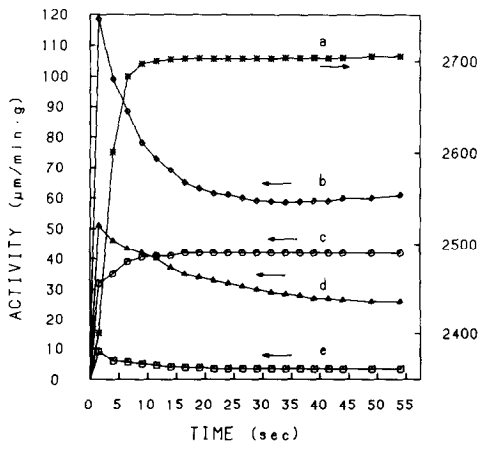

FIG. 3. Activity versus time for $Fe(CO)_5$/Y zeolite. Temperature = 285°C, 10% CO/H_2, 60-sec reaction. (a) CO, (b) CH_4, (c) CO_2, (d) C_2H_6, (e) C_3H_8, C_4H_{10}.

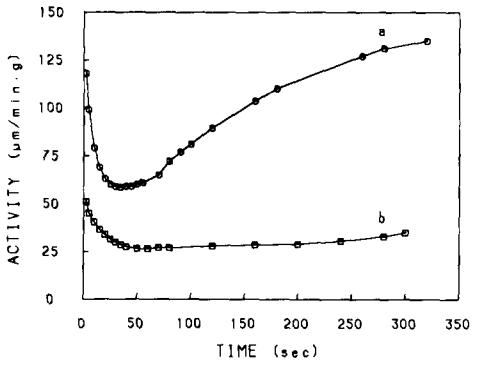

FIG. 4. Activity versus time for $Fe(CO)_5$/Y zeolite. Temperature = 285°C, 10% CO/H_2, 60-sec reaction. (a) CH_4, (b) C_2H_6.

hydrogen. After 1 min of reaction with 10% CO/H_2 over the $Fe(CO)_5$ Y zeolite sample (1) a 20-sec helium purge is made. The helium purge is followed by a hydrogen purge (30 ml/min) and the hydrogen reacts with surface carbon species and the surface is titrated. This desorption process yields information regarding the number, distribution, and activity of individual surface sites. A typical desorption curve in this case for sample 1 is shown in Fig. 5. The three types of sites which are labeled I, II, and III in Fig. 5 represent three CH_4 desorption sites.

If the 10% CO/H_2 mixture is changed to 10% CO/He then the surface species that are detected in a hydrogen titration desorption are quite different. In both cases, as time goes on more CH_4 is formed. However, the peak shape of the CH_4 production in the presence of CO/He is different, and only one distinct peak rather than three distinct peak shapes is observed. In both cases small amounts of C_2H_6 are desorbed. When CO/H_2 is used, more C_2H_6 and higher hydrocarbons are formed.

The activity for methane formation versus time can be studied as a function of temperature. The reaction rates double every 15°C as the 10% CO/H_2 mixture is passed over the zeolite catalysts. An activation energy for methane formation can be obtained from a plot of the log of the reaction rate versus the inverse of the temperature.

The bimetallic zeolite samples (2–5) were also studied as Fischer–Tropsch catalysts. The activation energies for methanation for samples 1–5 are reported in Table 4. Reaction product distributions, hydrogen titration desorption plots, and variable temperature activation plots were made for samples 2–5. Selected representative examples are reported in order to reflect the large variety of results obtained for these bimetallic systems.

Sample 2 reacted with a 10% CO/H_2 mixture to yield C_1 to C_4 products but the activity of this catalyst was low (4–8 μmole/g-min). The shape of the methanation activity curve indicates at least two contributions. The hydrogen titration desorption plot for sample 2 shows an initial CH_4 surge and then a decrease similar to the curve in Fig. 5 for sample 1. Evidence of two kinds of reaction intermediates is indicated by the peak shape of the desorption. Also, just as is the case for sample 1 the activity does not return to zero at long desorption times. Catalyst regeneration is needed for sample 2 after reaction times longer than 5 min. Regeneration of the catalyst is done by heating the catalyst in flowing hydrogen (30 ml/min) at 400°C for 5 min.

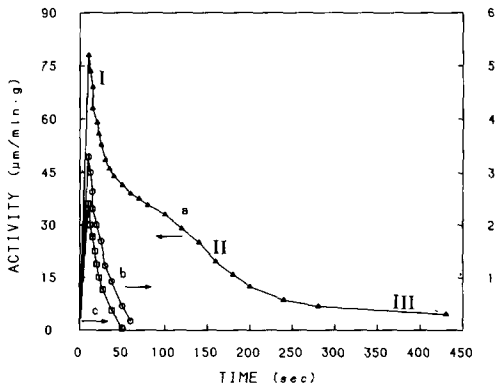

FIG. 5. Hydrogen titration, activity versus time for $Fe(CO)_5$/Y zeolite. Temperature = 285°C, 10% CO/H_2, 320-sec reaction, (a) CH_4, (b) C_2H_6, (c) C_3H_8, C_4H_{10}.

TABLE 4

Sample	Activation energy[a]	Number of sites	Percentage conversion[b]	C_1/C_{2+}	Bulk carbide[c]
1	98	2	10.5	2.4	Y
2	141	2[d]	2	2.2	Y
3	107	2	2	3.3	Y
4	110	1	9	2.5	N
5	91	1	5	3.8	N

[a] Activation energy for methane, kJ/mole.
[b] 285°C, 60-sec reaction, 10% CO/H_2, 30 ml/min, 25 mg sample.
[c] All carbides initially formed are ε', $Fe_{2.2}C$.
[d] Very noticeable, early formation of second site.

Sample 3 has about a 2% conversion and a C_1/C_{2+} ratio of about 3.3. The activity of sample 3 is also low (8–10 μmole/g-min.). The shape of the methanation activity plot indicates that there are at least two contributions. The desorption data show an initial CH_4 surge which decreases in time. Only CH_4 is detected during the hydrogen titration and at long reaction time the methanation activity does not return to zero.

The product conversion for sample 4 for reaction with 10% CO/H_2 at 285°C is about 9%. The C_1/C_{2+} ratio is approximately 2.5 at a quasi-steady state. Catalyst sample 3 has very high methanation activity and the corresponding activity versus time plot for 2 minutes is shown in Fig. 6. The hydrogen titration data indicate that the shape of the CH_4 desorption curve is independent of reaction time, that there is only one contribution under the curve and that the CH_4 activity does decrease to zero after long times (5 min).

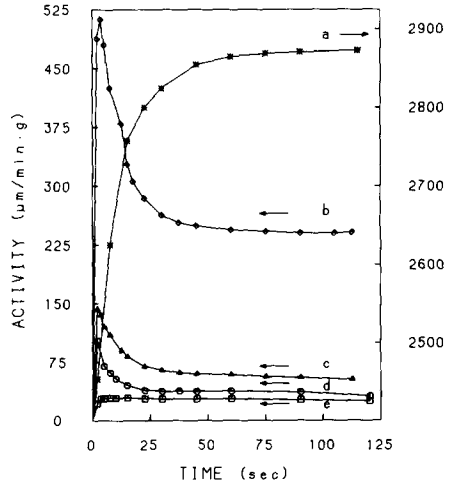

FIG. 6. Activity versus time for $Co^{2+}/[Fe(CN)_5NO]^{2-}/Y$ zeolite. Temperature = 285°C, 10% CO/H_2, (a) CO, (b) CH_4, (c) C_2H_6, (d) C_3H_8, (e) CO_2.

The percentage conversion for sample 5 is 5%. The ratio of C_1 to C_{2+} is about 3.8 at a quasi-steady state. The activity is good (between 120 and 200 μmole/g-min) for methane formation. Desorption hydrogen titration curves indicate that the amount of CH_4 depends on the 10% CO/H_2 reaction time but that only one contribution is present. The initial CH_4 surge decreases as reaction time increases. No other hydrocarbons besides CH_4 are formed during the hydrogen titration. Late in this reaction (after 10 min) the CH_4 activity comes to a steady state. If the 10% CO/H_2 is stopped and a helium stream is introduced a large amount of CO_2 is formed. Figure 7 shows the formation of the CO_2 when the syn gas mixture is switched to helium.

A comparison of samples 1–5 can be made by referring to Table 4. In Table 4 information concerning the relative methanation activity, a C_1/C_{2+} ratio, the number of contributions under the activity/desorption plot, the percentage conversion, and an indication of whether bulk carbide

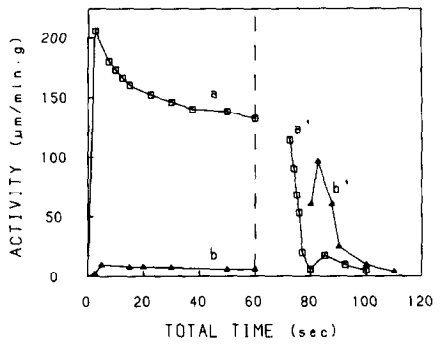

FIG. 7. Activity versus time for $Ru^{3+}/[Fe(CN)_5NO]^{2-}/Y$ zeolite. Temperature 285°C, 10% CO/H_2 stopped at 60 sec followed by He stream. (a) CH_4, (b) CO_2, (a') CH_4 after 10% CO/H_2 flow stopped, (b') CO_2 after 10% CO/H_2 flow stopped.

formation has been observed after reaction with the 10% CO/H_2 mixtures is assembled. The presence of bulk iron carbide was distinguished by the use of Mössbauer spectroscopy and X-ray powder diffraction experiments. An example of the use of Mössbauer spectroscopy to observe the formation of bulk iron carbide is shown in Fig. 8 for sample 1 after treatment with 10% CO/H_2 for 5 min at 285°C. Similar Mössbauer spectra that indicated the presence of bulk iron carbide formation were also obtained for samples 2 and 3.

DISCUSSION

A. Synthesis and Characterization of Zeolites before Reaction

The $Fe(CO)_5$ Y zeolite sample (1) is believed to contain $Fe(CO)_5$ units in the supercage of zeolite Y on the basis of our previous Mössbauer experiments (*8*), the infrared results presented in Table 3 and the infrared (*9, 19, 20, 26*) and spectroscopic work of others (*25*). Several researchers have suggested that the $Fe(CO)_5$ moiety (*9, 19*) as well as other metal carbonyl complexes (*20, 21*) are located in the supercages of zeolites X and Y. EPR studies and thermal analysis measurements (*21, 27*) also indicate that other metal carbonyls like $W(CO)_6$ remain intact with no carbonyl loss after initial sample preparation.

The reduction conditions for the $Fe(CO)_5$ Y zeolite, sample 1, are quite severe. Long thermal treatment (24 hr) under a very high hydrogen flow rate results in the observation of iron (0) as determined by Möss-

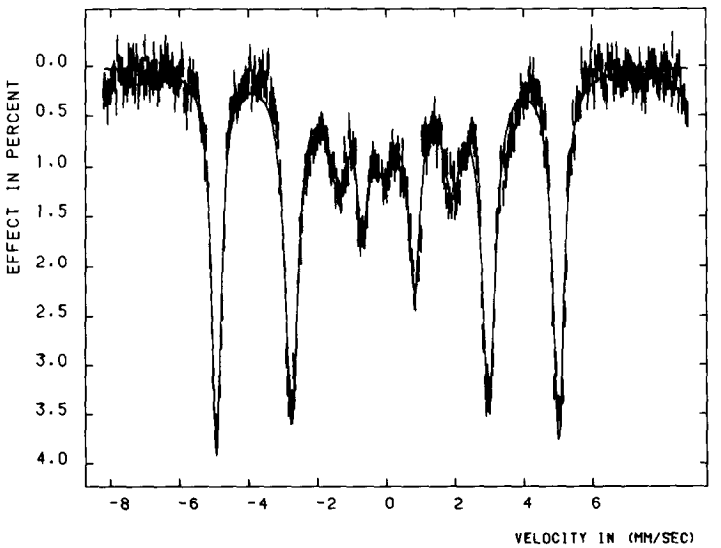

FIG. 8. Mössbauer spectrum of $Fe(CO)_5/Y$ zeolite indicating carbide formation, reaction time = 5 min, 10% CO/H_2, temperature = 285°C.

bauer spectroscopy. The Mössbauer spectrum in Fig. 2 indicates that the degree of reduction to the metallic state is high. Shorter reduction times and reduction in hydrogen at lower temperatures did not lead to the production of highly reduced iron (0) species.

Other supporting characterization studies of the $Fe(CO)_5$ Y zeolite as outlined in Table 3 indicate that the iron carbonyl containing zeolite is crystalline as determined by X-ray powder diffraction. This is not a surprising result, although iron ions in zeolites can cause disruption of the framework (*28*). The infrared bands reported in Table 3 are very similar to those reported for $Fe(CO)_5$ in NaY zeolite (*26*) and $Fe(CO)_5$ in HY zeolite (*9*). No bridging carbonyl bands are observed and this implies that larger clusters like $Fe_2(CO)_9$ and $Fe_3(CO)_{12}$ have not been formed under these conditions. ISS-SIMS experiments do not indicate segregation or large gradient concentration changes after depth profiling. This observation is in agreement with the Mössbauer results.

The synthesis and characterization of samples 2–5 are much more complex than sample 1. Samples 2–5 all have at least two transition metal components and several steps in their preparation. The infrared results of Table 3 provide evidence that the $[Fe(CN)_5NO]^{2-}$ anion is present to some extent in samples 2–5. The band at 2205 cm^{-1} is due to the CN^- frequency and the band at 1950 cm^{-1} corresponds to the NO frequency.

X-Ray results also show as with sample 1 that these materials are crystalline. The ISS-SIMS results indicate that both the metals incorporated by the ion-exchange and by the nitroprusside complex are present although there is only a small amount of iron as detected by SIMS. This observation is in agreement with the Mössbauer results of Table 2 since no Mössbauer signal was observed for the ruthenium nitroprusside Y zeolite, sample 5. Our Mössbauer source is not exceedingly strong (85 mCi) and with a stronger source a Mössbauer spectrum for sample 5 might be obtained.

On the other hand, it was pointed out earlier that alkali metals and alkaline earths do not seem to bind to either the nitroprusside anion or hexacyanoferrate (II) or hexacyanoferrate (III) anions. Further studies from our laboratory with transition metal ions of a 3^+ or 4^+ charge (Co^{3+}, Pt^{4+}) also indicate that little or no binding of these iron anionic complexes occurs when the types of cations have been exchanged into the zeolite.

The exact nature of the complexation of the anionic iron complex to cations in the zeolite is not well known. It is likely that complexation initially occurs by an inner sphere mechanism involving cyanide bridging groups. The charge balance involved in this reaction is not totally understood but could deal with dealumination of the lattice, although aluminum ions in solution and broadened X-ray peaks have not been observed (*40*). Since complexation does not occur with alkali metals or alkaline earths or certain transition metals, the size, charge, and polarizability of the exchanged transition metal cation determine whether complexation will or will not occur. Significant amounts of iron are present in samples 2–4 as indicated by microanalyses and by Mössbauer experiments.

B. Characterization after Reduction, during Reaction, and after Reaction

1. Mössbauer. The Mössbauer spectrum of a $CoNH_4Y$ sample after complexation with nitroprusside and reduction under flowing hydrogen as shown in Fig. 1 indicates that the iron is highly reduced. Samples 2 and 3 are similar. Before reduction the Mössbauer isomer shifts and quadrupole splittings are very close to that of sodium nitroprusside (*8, 29*). After reduction the iron is reduced to the iron (0) state. Analysis of the area under peaks indicate that sample 3 is totally reduced and that samples 2 and 4 are 90 and 95% reduced to iron (0), respectively.

The hyperfine field strengths of samples 2–4 as reported in Table 2 indicate a range between 320.4 and 331.3 kOe. These should be compared to a value of 333 kOe for alpha-iron (0). This indicates that there is no alloying occurring in these catalysts. XPS experiments of the copper zeolite, sample 2, show that the copper has not been reduced to copper (0) but to copper (I).

The isomer shift for sample 1 before reduction, however, is not consistent with matrix isolation Mössbauer studies of $Fe(CO)_5$ as has been pointed out earlier by us (*8*). This isomer shift may be an indication of oxidation of the iron but carbonyl ligands are definitely present and the infrared data in Table 3 are indicative of $Fe(CO)_5$ as reported by other researchers (*9, 19, 20, 26, 32*). The effect of the other metal in the bimetallic system besides iron seems to only affect the hyperfine field strength values in the case of the copper and zinc samples (*2, 3*). At the present time we do not understand why these hyperfine field strength values are smaller than in the case of α-Fe and other bimetallic zeolite catalysts that we have investigated (*8*).

Stanfield and Delgass (*39*) have studied mixed cobalt iron silica catalysts and reported the Mössbauer characteristics for FeCo alloys. Based on their observations of increased hyperfine field strength for CoFe alloys with respect to α-iron there is no alloying in our cobalt iron sample (*4*). Another observation of Stanfield and Delgass (*39*) is that a lower extent of carburization occurs during Fischer–Tropsch synthesis for low cobalt concentrations which may also be an important factor in understanding the catalytic behavior of sample 4.

2. *X-ray powder diffraction data.* The X-ray powder diffraction data as summarized in Table 3 indicate that these samples are crystalline before and after reduction and that extra peaks for α-Fe occur after reduction of the samples except for sample 5. The bimetallic samples might be expected to show extra peaks after reduction for metal or metal oxide phases. In the case of sample 2 no evidence of metallic copper is indicated in the powder pattern although microanalyses and surface analyses indicate that copper is indeed present. Sample 3 after reduction has an X-ray powder diffraction pattern that indicates that metallic zinc is not present and perhaps that a zinc-oxide phase is present as evidenced by a peak at 34.5°2θ. However, main peaks reported for ZnO at 36.2°2θ and 31.7°2θ are not observed. The X-ray powder diffraction pattern of sample 4 which contains cobalt does show a weak peak at $2\theta = 65.9°$ which is an indication of β-Co. Peaks for cobalt (II) or (III) oxides were not observed. Last of all, sample 5 shows an X-ray powder diffraction pattern that has a peak at 55.5°2θ indicative of RuO_2.

3. *Particle sizes and reduction conditions.* The reduction conditions for the bimetallic zeolites samples, 2–5, are much less harsh than for sample 1. In comparison to the reduction of other iron-containing zeolites (*1, 3–8, 13*) the conditions used here are mild. This observation should be of importance in the design of other bimetallic catalysts. For instance, other potentially volatile species like HCl could be generated if Cl^- ions are present.

Zeolite materials that we have studied that contain iron *cations* do not readily reduce to the metallic state even if these iron cations are complexed to the anionic iron species. This observation is in excellent agreement with others (*1, 3–8, 13*).

The location of the transition metals and the dispersion of these reduced materials are not totally understood, but the X-ray powder diffraction and scanning and transmission electron microscopy experiments indicate that the iron (0) species are not highly dispersed. These observations are in conflict with another report (*2*) but it is possible that there are differences in the synthetic procedure or starting materials that could account for this difference.

B. Activity, Selectivity and Stability of These Catalysts

1. Sample 1. The catalytic activity of the $Fe(CO)_5Y$ zeolite, sample 1, shows a high percentage conversion. The product distributions of both Figs. 3 and 4 indicate that there is no steady state. This means that the surface is changing throughout the reaction. The observation that there is an increase of CH_4 with respect to larger hydrocarbons such as C_2H_6 at larger reaction time also indicates that changes in surface states are occurring. New active carbon sites are forming on the catalyst surface in time.

In relation to the selectivity of this catalyst, the amount of methane produced is about twice that of the C_{2+} hydrocarbons. The amount of CO_2 produced is approximately one-half of the total amount of hydrocarbons.

The hydrogen titration data of Fig. 5 indicate that there are several sites for methane formation. The first site is very active but short-lived. The shoulder implies that a second site starts to form later in the reaction. A third site is implied by the observation that the activity does not return to zero. This third site is believed to be due to the formation of bulk iron carbide. Further support for the formation of bulk iron carbide formation is given in the Mössbauer spectrum shown in Fig. 8. X-ray powder diffraction provides evidence that the initial carbide is of the ε' form which has the stoichiometry $Fe_{2.2}C$.

Reaction of sample 1 with 10% CO/He provides evidence that the catalyst is being deactivated in time. Since the hydrogen titration curve, which yields information about the surface sites, is very different in shape when 10% CO/He is used instead of 10% CO/H_2 this indicates that H_2 is very important in the formation of the active surface states that are believed to exist. Since the shape of the CH_4 peak changes in time for the hydrogen titration with 10% C_2H_4/He this implies that the activity of the catalyst is changing in time. It is clear that the surface of this zeolite catalyst is in a state of fluctuation. The methanation activation energy is 98 μmole/g-min.

2. Samples 2–5. The samples described in Table 1 do not all contain the same loadings of metals. The $Fe(CO)_5$ sample contains 5% by weight of iron. Sample 2 contains a small amount of copper ions before reduction because there are relatively few available ion-exchange sites in ZSM-5. The corresponding amount of iron from the nitroprusside anion is also low. XPS measurements reveal that the amounts of Cu^{2+} and Fe^{3+} in sample 2 are both less than 1%. The Zn^{2+}, Co^{2+}, and Ru^{3+} concentrations for samples 3 through 5, respectively, are higher than the amount of Cu^{2+} in sample 2. XPS measurements on each of these samples indicate that these ions are present at about 3%. The amount of iron ions from nitroprusside in samples 3 and 4 is fairly high (2%) based on XPS measurements but the amount of iron in sample 5 is very low (<1%). These relative concentrations should give the reader an idea of the relative levels of metal surface content of these samples. The bimetallic zeolite catalysts have quite different activities and selectivities and will be individually discussed below.

Sample 2 contains iron and copper ions. This catalyst shows low activity for methanation and for other larger hydrocarbons. A variety of products were obtained and several active sites are believed to exist on the surface. The hydrogen titration of this catalyst implies that there are two kinds of reaction intermediates and that the first site is readily deactivated. Some bulk iron carbide of the ε' form exists as evidenced by Mössbauer spectroscopy and X-ray powder diffraction experiments. Some inactive carbon deposits are present on the surface since this catalyst needed to be regenerated after short (5 min) reaction time.

The zinc nitroprusside Y reduced zeolite, sample 3, is the most readily reduced sam-

ple that we have studied. The percentage conversion and activity, however, are very low. The reaction of 10% CO/H_2 with sample 3 indicate two kinds of surface carbon sites and the hydrogen titration data also support this suggestion. The first site which is observed in the hydrogen titration desorption experiment is readily deactivated. The absence of other hydrocarbons besides CH_4 does not mean that other hydrocarbons are not formed. The percentage conversion is so low with this catalyst that higher molecular weight hydrocarbons (C_{3+}) may just not be detectable. Bulk iron carbide formation is implied by the hydrogen titration and indeed was detected in a Mössbauer experiment. Catalyst regeneration was necessary to destroy inactive carbon deposits that built up on the surface.

As observed in Fig. 6, sample 4 has a high percentage conversion and a high activity. Only one kind of surface site is present as suggested by the hydrogen titration desorption. Since the CH_4 activity continually increases with time there must be some surface rearrangement. The hydrogen titration desorption data imply that there is no bulk iron carbide formation and none was detected in either Mössbauer or X-ray powder diffraction experiments. This catalyst is a very good methanation catalyst. This observation is in good agreement with other methanation studies of cobalt-containing zeolite catalysts (*22*).

When ruthenium cation-exchanged zeolites are complexed with nitroprusside and reduced, the activity is good. The shape of the hydrogen titration, however, indicates only one kind of surface site. Also, the only detected product during the hydrogen titration is CH_4 but mass spectral data indicate that larger hydrocarbons are formed. In time the CH_4 activity comes to a steady state implying that surface carbon species do not all convert to inactive carbon. The observation of large amounts of CO_2 during the helium purge, shown in Fig. 7, implies that carbonyl groups on the metal sites are reacting with oxygen sites on nearby metal sites.

C. The Nature of Surface Carbon Species

A detailed mechanism of the buildup of carbon species on the surface of alumina (*38*) under similar conditions used in this study indicates that in the case of samples 1, 2, and 3 studied here that the nature of the surface carbon species are very similar to that on alumina. The CH_4 curve of Fig. 5 can be deconvoluted into three peaks. The first sharp peak is believed to be a surface carbon species which has hydrogen associated with it. Evidence for hydrogen content comes from an oxygen titration of the surface. The second peak which appears as a shoulder is due to a surface carbide species. Finally, the activity does not return to zero and therefore the third broad flat band is due to bulk carbide which forms later in the reaction. Evidence of the bulk carbide also comes from Mössbauer experiments such as the one observed in Fig. 8. We propose that the second peak may form only if the bulk carbide eventually forms and that it is a precursor to bulk carbide formation. In the case of samples 4 and 5 both the second peak and a bulk carbide phase never form.

D. Summary

The following conclusions have been made concerning these catalysts:

1. The selectivity, activity, and thermal stability of these zeolite catalysts can be controlled by incorporating combinations of transition metals. Methanation activation energies range from 91 to 141 kJ/mole.

2. Deviation from Schulz–Flory kinetics (*30*) can be realized by choice of the metal, zeolite, synthesis gas composition, and temperature. Pressure is also an important factor that has not been varied in our studies. A long hold-up time for higher molecular weight components in zeolites also can contribute to the impression that deviations from Schulz–Flory behavior are occurring. In two component systems (*31, 33*) such as ours the zeolite can provide a

shape selectivity function and a metal like iron provides the ability to reduce CO.

3. Metallic particles are large (from 50 to 150 Å) on the outside of the zeolites. The presence of two metals influences the C_1/C_{2+} ratio. For example, when Ru is present a high C_1/C_{2+} ratio is found. The C_1/C_{2+} ratio for these zeolites is lower (2.2–3.8) than that for iron on alumina (5.1) (*37*).

4. Initial bulk iron carbide formation is of the ε' type. This observation has been made for iron on other supports (*11, 34, 36*) for temperatures lower than 300°C. The χ iron carbide phase was observed after 10-min reaction times for samples 2 and 3. Bulk carbide formation does not occur when Ru^{3+} or Co^{2+} ions are ion-exchanged into the zeolite.

ACKNOWLEDGMENTS

S. L. S. and K. C. M. thank the donors of the Petroleum Research Fund, administered by the American Chemical Society and the University of Connecticut Research Foundation for support of this research.

REFERENCES

1. Lee, J. B., *J. Catal.* **68,** 27 (1981).
2. Scherzer, J., and Fort, D., *J. Catal.* **71,** 111 (1981).
3. Lo, C., Rao, K. R. V. M., Mulay, L. N., Rao, V. U. S., Obermyer, R. T., and Gormley, R. J., *Adv. Chem. Ser.* **194,** 573 (1981).
4. Ballivet-Tkatchenko, D., and Tkatchenko, I., *J. Mol. Catal.* **13,** 1 (1979).
5. Nagy, J. B., van Eenoo, M., and Derouane, E. G., *J. Catal.* **58,** 230 (1979).
6. Gunsser, W., Adolph, J., and Schmidt, F., *J. Magn. Magn. Mat.* **15,** 1115 (1980).
7. Gager, H. M., and Hobson, M. C., Jr., *Catal. Rev.* **11,** 117 (1975).
8. Suib, S. L., McMahon, K. C., and Psaras, D., *in* "Intrazeolite Chemistry" (G. D. Stucky and F. G. Dwyer, Eds.), ACS Symposium Series, pp. 218, 301–318. American Chemical Society, Washington, D.C., 1983.
9. Ballivet-Tkatchenko, D., and Coudurier, G., *Inorg. Chem.* **18,** 558 (1979).
10. For an excellent review of proposed Fischer–Tropsch mechanisms refer to ref. *11* and references therein.
11. Rofer-Depoorter, C. K., *Chem. Rev.* **81,** 447 (1981).
12. Nijs, H. H., Jacobs, P. A., and Uytterhoeven, J. B., *J. Chem. Soc. Chem. Commun.* 180 (1979).
13. Obermyer, R. J., Mulay, L. N., Lo, C., Oskooie-Tabrizi, M., and Rao, V. U. S., *J. Appl. Phys.* **53,** 2683 (1982).
14. Bennett, C. O., *in* "Catalysis under Transient Conditions" (A. T. Bell and L. L. Hegedus, Eds.), ACS Symposium Series, No. 178, pp. 1–32. American Chemical Society, Washington, D.C., 1982.
15. Chrismon, B. L., and Tumolillo, T. A., *Comp. Phys. Commun.* **2,** 322 (1971).
16. Delgass, W. N., and Chen, L. Y., *Rev. Sci. Instrum.* **47,** 968 (1976).
17. Suib, S. L., Zerger, R. P., Stucky, G. D., Emberson, R. M., Debrunner, P. G., and Iton, L. E., *Inorg. Chem.* **19,** 1858 (1980).
18. Suib, S. L., Coughlin, D. F., Otter, F. A., and Conopask, L., *J. Catal.* **84,** 410 (1983).
19. Bailey, D. C., and Langer, S. H., *Chem. Rev.* **81,** 109 (1981).
20. Abdo, S., Gosbee, J., and Howe, R. F., *J. Chim. Phys.* **78,** 885 (1981).
21. Gallezot, P., Coudurier, G., Primet, M., Imelik, B., *in* "Molecular Series II" (J. R. Katzer, Ed.), ACS Symposium Series 140, pp. 144–149. American Chemical Society, Washington, D.C., 1976.
22. (a) Abdulahad, I., and Relek, M., *Erdol Konle, Erd gas, Petrochem. Brennstoff. Chem.* **25,** 187 (1972). (b) Lapidus, A. L., Isakov, Ya. I., Guseva, I. V., Minachev, Kh. M., and Eidus, Ya. T., *Izv. Akad. Nauk SSSR, Ser. Khim.* 1441 (1974). (c) Vanhove, D., Makambo, P., and Blanchard, M., *J. Chem. Soc. Chem. Commun.* 605 (1979). (d) Fraenkel, D., and Gates, B. C., *J. Amer. Chem. Soc.* **102,** 2478 (1980).
23. Argauer, R. J., and Landolt, G. R., U.S. Patent 3,702,886 (1972).
24. Fergusson, J. E., and Love, J. L., *Inorg. Synth.* **13,** 208 (1971).
25. Gallezot, P., Coudurier, G., Primet, M., and Imelik, B., *in* "Molecular Sieves II" (J. R. Katzer, Ed.), pp. 144–155. ACS Symposium Series 40, American Chemical Society, Washington, D.C., 1976.
26. Bein, Th., Jacobs, P. A., and Schmidt, F., *in* "Metal Microstructures in Zeolites" (P. A. Jacobs, N. I. Jaeger, P. Jiru, and G. Schulz-Ekloff, Eds.), Vol. 12, pp. 111–121. Elsevier, New York, 1982.
27. Rommelfaenger, P., and Howe, R. F., *J. Chem. Soc. Chem. Commun.* 123 (1979).
28. Delgass, W. N., Garten, R. L., and Boudart, M., *J. Chem. Phys.* **50,** 4603 (1969).
29. Epstein, L. M., *J. Chem. Phys.* **36,** 2731 (1962).
30. Henrici-Olive', G., and Olive', S., *Angew. Chem. Int. Ed.* **15,** 136 (1976).
31. (a) Hagg, W. O., and Huang, T. J., U.S. Patent 9,157,338 (1979). (b) Chang, C. D., Lang, W. H., and Silvestri, A. J., Belg. Patent 463,711 (1974).
32. Ballivet-Tkatchenko, D., Coudurier, G., Moz-

zanega, H., and Tkatchenko, I., *Fundam. Res. Homog. Catal.* **3,** 257 (1981).
33. Jacobs, P. A. *in* "Catalysis by Zeolites" (B. Imelik, C. Naccache, Y. B. Taarit, J. C. Vedrine, G. Coudurier, and H. Praliaud, Eds.), Vol. 5, pp. 293–308. Elsevier, New York, 1980.
34. Cäer, G. L., Dubois, J. M., Pijolat, M., Perrichon, V., and Bussiere, P., *J. Phys. Chem.* **86,** 4799 (1982).
35. Amelse, J. A., Grynkevich, G., Butt, J. B., and Schwartz, L. H., *J. Phys. Chem.* **85,** 2484 (1981).
36. Niemansverdriet, J. W., van der Kaan, A. M., van Dijk, W. L., and van der Baan, H. S., *J. Phys. Chem.* **84,** 3363 (1980).
37. Bianchi, D., Borcar, S., Teule-Gay, F., and Bennett, C. O., *J. Catal.* **82,** 442 (1983).
38. Bianchi, D., Tau, L. M., Borcar, S., and Bennett, C. O., *J. Catal.*, submitted.
39. Stanfield, R. M., and Delgass, W. N., *J. Catal.* **72,** 37 (1981).